In Situ Phosphorus-Doped Polycrystalline Silicon Films by Low Pressure Chemical Vapor Deposition for Contact Passivation of Silicon Solar Cells

Meriç Fırat[a,b,*], Hariharsudan Sivaramakrishnan Radhakrishnan[b], María Recamán Payo[c], Filip Duerinckx[b], Loic Tous[b], Jef Poortmans[a,b,d]

[a]*KU Leuven, Department of Electrical Engineering, Kasteelpark Arenberg 10, 3001 Leuven, Belgium*
[b]*Imec (Partner in EnergyVille), Kapeldreef 75, 3001 Leuven, Belgium*
[c]*KU Leuven, Department of Physics and Astronomy, Celestijnenlaan 200d, 3001 Leuven, Belgium*
[c]*UHasselt, 3590 Diepenbeek, Belgium*

[*]Corresponding author: meric.firat@imec.be

Abstract – *In situ* phosphorus (P)-doped polycrystalline silicon (poly-Si) films by low pressure chemical vapor deposition (LPCVD) were studied in this work for the fabrication of poly-Si passivating contacts. *In situ* doping was targeted for enabling the full potential of the high-throughput LPCVD technique, as it could allow leaner fabrication of industrial solar cells featuring poly-Si passivating contacts than the more common *ex situ* doping routes. By careful optimization of the deposition temperature and the flows of the carrier gas (H_2) and the dopant precursor (PH_3), high doping in the poly-Si layers was achieved with active P concentrations up to $1.3 \cdot 10^{20}$ cm^{-3}. While reduction in the deposition rate (r_{dep}) and thus in the throughput is a known problem when growing *in situ* P-doped films by LPCVD, this reduction could be limited, and the resulting r_{dep} was equal to 0.078 nm/s. The developed poly-Si films were characterized both structurally and in terms of their passivation potential in poly-Si contacts. The latter yielded recombination current densities down to 1.5 fA/cm^2 in passivated ($J_{0,p}$) and 25.6 fA/cm^2 in screen-printing metallized ($J_{0,m}$) regions on saw-damage removed (SDR) Cz-Si surfaces, respectively, accompanied by a contact resistivity ($\rho_{c,m}$) of 4.9 m$\Omega \cdot$cm^2. On textured Cz-Si surfaces, the corresponding values were $J_{0,p}$ = 3.5 fA/cm^2, $J_{0,m}$ = 56.7 fA/cm^2, and $\rho_{c,m}$ = 1.8 m$\Omega \cdot$cm^2. Optical impact of the developed poly-Si films was also assessed and a short circuit density loss of 0.41 mA/cm^2 is predicted per each 100 nm of poly-Si applied at the rear side of solar cells.

Keywords – passivating contacts, solar cells, polysilicon, LPCVD, *in situ* doping, phosphorus doping

1 Introduction

The silicon (Si) photovoltaics (PV) industry is currently dominated by the passivated emitter rear cell (PERC) technology (Fischer et al., 2021), which is reaching its limits due to high contact recombination dominating the cell performance (Yan et al., 2021). Thus, passivating contacts are widely considered as the next technological development to be applied to state-of-the-art Si solar cells for further power conversion efficiency (η) improvements (Fischer et al., 2021). Among several competing technologies, contact passivation based on a stack of heavily doped polycrystalline silicon (poly-Si) and ultrathin silicon oxide (SiO_x) films has received a particularly high level of interest and acceptance both in the PV research community and industry. As a result, a record efficiency of 26.1% (Haase et al., 2018) and average production efficiencies of 24% (Chen et al., 2021; Xiao, 2020) have already been demonstrated for solar cells incorporating these poly-Si passivating contacts.

The promise and the rapid adoption of poly-Si passivating contacts follow from a few advantageous properties: (i) excellent electrical properties in terms of effective repelling of minority carriers and transport of majority carriers to the contacts, which allow the simultaneous achievement of low recombination current density (J_0) and contact resistivity (ρ_c) values (see Fig. 1), (ii) compatibility with standard high-temperature processes in existing PV production lines, and (iii) reliance on conventional materials which have the potential to be fabricated by lean process flows, with a high throughput (Chen et al., 2019; Feldmann et al., 2018; Yan et al., 2021). The latter aspect is particularly important for achieving a low levelized cost of electricity with solar cells incorporating poly-Si passivating contacts and is therefore the focus of this work.

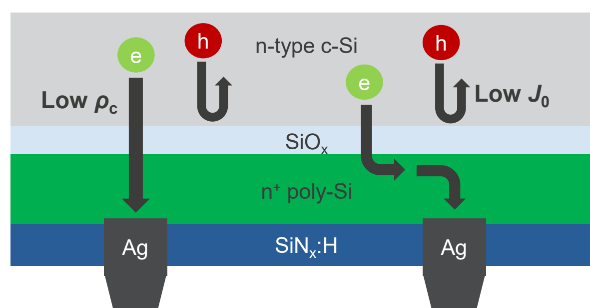

Figure 1. Schematic of a typical n-type poly-Si passivating contact structure at the rear side of an industrial n-type silicon solar cell with screen-printed contacts. Repelling of the minority carriers i.e., holes (h) by the passivating contact leads to a low recombination current density (J_0). Effective extraction of the majority carriers i.e., electrons (e) to the contacts yields a low contact resistivity (ρ_c).

For fabrication of the poly-Si/SiO_x structure used for contact passivation, various industrially viable approaches have been proposed in the literature, with the two main techniques for realizing the poly-Si film being low pressure chemical vapor deposition (LPCVD) and plasma enhanced chemical vapor deposition (PECVD) (Yan et al., 2021). Among these options, the primary choice of the PV industry has been the use of LPCVD systems so far (Fischer et al., 2021). This is motivated by (i) the high wafer throughput of LPCVD equipment, (ii) the simplicity of realizing over 100 nm thick blister-free poly-Si films (Yan et al., 2021), and (iii) the possibility of growing the ultrathin SiO_x film *in situ*, by thermal oxidation before poly-Si deposition. Nevertheless, the LPCVD-based approach which is currently common in the PV industry and research community is still inherently a two-step process despite the *in situ* oxidation. This is because the high level of doping required in the poly-Si film is obtained by an *ex situ* doping step, either by diffusion or ion implantation of dopants (Yan et al., 2021). Dopant diffusion consists of deposition of a dopant-rich layer followed by a dopant drive-in process, and thus can be quite time-consuming, while ion implantation requires an extra annealing step for the activation of the implanted dopants. Hence, the choice of *ex situ* techniques for doping complicates the fabrication by LPCVD. This is an important disadvantage in comparison to the competing PECVD-based approach, which mostly relies on *in situ* doping (Feldmann et al., 2018). The promise of the simpler *in situ* approach is also reflected in recent market predictions, which forecast a significant increase in the market share of this doping method (Fischer et al., 2021).

This work proposes a leaner LPCVD-based process for the fabrication of poly-Si films for contact passivation, by performing *in situ* doping during poly-Si growth. Particularly, phosphorus (P)-doped films are studied, as n-type poly-Si passivating contacts have shown more promise and found more acceptance by the PV industry than their p-type counterparts (Feldmann et al., 2018; Yan et al., 2021). The proposed *in situ* approach offers two potential advantages compared to the standard *ex situ* doping methods. First, the need for extra doping steps becomes obsolete, allowing for simpler fabrication of solar cells with poly-Si passivating contacts. Second, tuning of the thickness of *in situ* doped poly-Si films without altering the doping level can be achieved in a more straightforward manner, by a simple adjustment of the deposition duration. By contrast, changes in the thickness of *ex situ* doped poly-Si films would require the doping process, e.g. diffusion of dopants, to be reoptimized to preserve the original doping profile. The simplicity of poly-Si thickness modification could be useful for the PV industry to achieve evolutionary increases of solar cell efficiencies by reducing the poly-Si

thickness and thus the associated free carrier absorption (FCA) related optical losses (Fırat et al., 2019).

The proposal of combining LPCVD with *in situ* P-doping, however, needs to address the challenges this approach faces, because of which *ex situ* P-doping methods have been prevalent so far. These challenges are the result of the complications arising from introducing the dopant precursor phosphine (PH_3) during the LPCVD process. The first issue is that a trade-off exists between the active P concentration ($N_{D,act}$) in the poly-Si films, which needs to be typically above $1 \cdot 10^{20}$ cm^{-3} for achieving low J_0 and ρ_c values, and the deposition rate (r_{dep}) (Kamins, 1998). Since fabrication of heavily *in situ* P-doped poly-Si films by LPCVD with a high throughput has also been of interest in the field of Si microelectronics, a vast amount of research has already been devoted to better understanding and addressing this trade-off. It was found that a higher deposition temperature (T_{dep}) yields a higher r_{dep}, as the Si precursor silane (SiH_4) decomposes quicker, but simultaneously a lower $N_{D,act}$, since desorption rate of PH_3 from the film surface increases (Learn and Foster, 1987). Moreover, it was shown that increasing the PH_3 flow (Q_P) enhances $N_{D,act}$, as more P is incorporated in the poly-Si, while it reduces r_{dep}, since PH_3 competes with SiH_4 for adsorption at available surface sites and thereby inhibits film growth (Meyerson and Yu, 1984; Mulder et al., 1990). Furthermore, importance of post-LPCVD annealing for grain growth and dopant activation i.e., $N_{D,act}$ enhancement was demonstrated (Ahmed and Ahmed, 1992; Mulder et al., 1990). In addition, use of disilane (Si_2H_6) instead of silane as the Si precursor was investigated as a strategy to enhance r_{dep} of *in situ* P-doped LPCVD poly-Si films (Grahn et al., 1997; Madsen and Weaver, 1990). Based on this knowledge, this paper addresses the problem concerning the trade-off by targeting the optimal balance between $N_{D,act}$ and r_{dep} specifically for application of the *in situ* P-doped LPCVD poly-Si films in passivating contacts for Si solar cells. The second challenge of combining LPCVD with *in situ* doping is the difficulty of depositing highly uniform poly-Si films in terms of thickness and doping level, which was also studied by Si microelectronics researchers (Ahmed and Ahmed, 1992; Meyerson and Olbricht, 1984). While discussion of this second problem is beyond the scope of this paper, Naber et al. (2019) has already reported an industrial *in situ* P-doped LPCVD solution which demonstrates the fabrication of highly uniform poly-Si films for passivating contacts, and thus, together with the findings of this work, the potential of this manufacturing route for the PV industry.

This paper reports on a systematic investigation of the impact of LPCVD process parameters on *in situ* doped poly-Si properties, with the aim of achieving a high $N_{D,act}$ while minimizing the drop in r_{dep} compared to the growth of undoped films. Findings of thorough structural and electrical characterization performed throughout this investigation are presented. Moreover, the resulting poly-Si films are incorporated in a poly-Si passivating contact structure, the potential of which is studied by assessing the J_0 and ρ_c values obtainable.

2 Materials and Methods

The work on the LPCVD-based *in situ* P-doping process was performed in four stages: (i) study and development of the poly-Si films, (ii) investigation of the impact of a post-LPCVD annealing process on the developed films, (iii) assessment of the performance of these films in passivating contacts, and (iv) characterization of the optical impact of the films when used at the rear side of a typical Si solar cell structure.

2.1 Development of *In Situ* P-Doped LPCVD Poly-Si Films

The film development was undertaken in a single-wafer ASM Epsilon 2000 reactor. The *in situ* P-doped poly-Si films were prepared by LPCVD using 100% SiH_4 as the Si precursor, 0.1% PH_3 diluted in H_2 as the dopant precursor, and H_2 as the carrier gas, on mirror-polished single crystalline Si (c-Si) substrates with a 100 nm thick thermally grown SiO_2. No post-LPCVD annealing was applied to these samples.

Starting with the baseline process shown in Table 1, the development consisted of studying the impact of (i) the T_{dep}, (ii) the level of dilution with the carrier gas i.e., the H_2 flow (Q_H), and (iii) the Q_P, on $N_{D,act}$, r_{dep}, and further structural properties of the poly-Si films. The pressure (p) and the flow of the Si precursor (Q_S) were not changed. The complete list of the process parameters used during the film development is presented in Table 1.

Table 1. The process parameters used for the growth of the *in situ* phosphorus-doped polycrystalline silicon films by low pressure chemical vapor deposition, at various stages of the film development.

Parameter Studied	p [Torr]	T_{dep} [°C]	Q_H [slm]	Q_P [sccm]	Q_S [sccm]
Baseline Process	40	700	25	500	200
T_{dep}	40	550-720	25	500	200
Q_H	40	590, 650, 700	15, 25	500	200
Q_P	40	590	10	0-300	200

The carrier concentration and thereby the $N_{D,act}$ in the poly-Si films was determined by Hall measurements, which also provided the Hall mobility of electrons ($\mu_{H,n}$). The total concentration of P (N_D) in the films was assessed by secondary-ion mass spectroscopy (SIMS). Using the depth-resolved profiles of N_D acquired by SIMS, average values of N_D in poly-Si films were calculated. For determining r_{dep}, poly-Si film thickness (t_{poly}) was measured by spectroscopic ellipsometry and divided by the deposition duration. A t_{poly} of 150 nm was targeted for all films but not achieved always as r_{dep} was often unknown prior to the depositions. Hence, t_{poly} of the films varied between 20 nm and 600 nm.

The poly-Si films were also characterized structurally by Raman spectroscopy, X-ray diffraction (XRD), and cross-section transmission electron microscopy (TEM). The Raman spectra were used for qualitative assessment of the crystallinity of the films under study. The XRD results were quantitatively analyzed by extracting the full width at half maximum of the peak related to (111)-oriented crystallites, and subsequently determining the crystallite size of the poly-Si films by utilizing the Debye-Scherrer equation (Langford and Wilson, 1978). The TEM images were used for a qualitative assessment of the grain size of the poly-Si films (Joubert et al., 1987).

2.2 Impact of Annealing on the *In Situ* P-Doped LPCVD Poly-Si Films

To study the impact of post-LPCVD annealing on the developed *in situ* P-doped poly-Si films, samples with the same design as described in Section 2.1 were prepared, using T_{dep} = 590°C, Q_H = 10 slm, and Q_P = 200 sccm. In a first experiment, the samples were subjected to 30 min long anneals at annealing temperatures of 800°C and 900°C, in the LPCVD equipment used for poly-Si deposition, in an airtight H_2 ambient, at 40 Torr or atmospheric pressure.

Subsequently, two samples were prepared and annealed at 900°C for 30 min in a different furnace which is not airtight, at atmospheric pressure. One of these samples was annealed in an O_2 ambient and the other in an N_2 ambient. The poly-Si film of the latter sample was covered with a 1.4 nm thick SiO_x layer grown wet-chemically in an ozonated H_2O bath, prior to annealing. The samples from both experiments were investigated by SIMS and Hall measurements. Moreover, the poly-Si films were characterized structurally by Raman spectroscopy and XRD measurements.

2.3 Development of Poly-Si Passivating Contacts

The aim of the third stage of development in this work was to determine the process window and choices allowing the highest passivating contact quality in terms of J_0 and ρ_c. For this purpose, symmetrical samples were fabricated as illustrated in Fig. 2a), following the process flow in Fig. 2b). The quality of the passivating contacts was assessed both on saw-damage removed (SDR) and random-pyramid textured (TXT) wafers. The parameters of these substrates are shown in Fig. 2a). These wafers were cleaned and thermally oxidized with a 1.3 nm thick SiO_x layer. Following the oxidation, the developed *in situ* P-doped poly-Si films were deposited by LPCVD, using the selected parameters: T_{dep} = 590°C, Q_H = 10 slm, and Q_P = 200 sccm. The samples were then subjected to the post-LPCVD annealing process, designed according to the results of the study on the impact of annealing on the poly-Si films. This consisted of coating the samples with a wet-chemical SiO_x film and annealing in an N_2 ambient, in a furnace which is not airtight. After annealing, the samples were hydrogenated by deposition of ~80 nm thick PECVD SiN_x:H films onto the poly-Si films. The fabrication was completed by screen-printing Ag fingers onto one side of the samples, followed by drying and firing-through of the Ag paste for contacting the poly-Si film. Firing was performed in a belt furnace with a speed of 150 inches per minute and a set peak temperature (T_{peak}) adapted to the wafer surface morphology. T_{peak} was chosen as 870°C for SDR and as 840°C for TXT samples, as the TXT wafers absorb and heat up more.

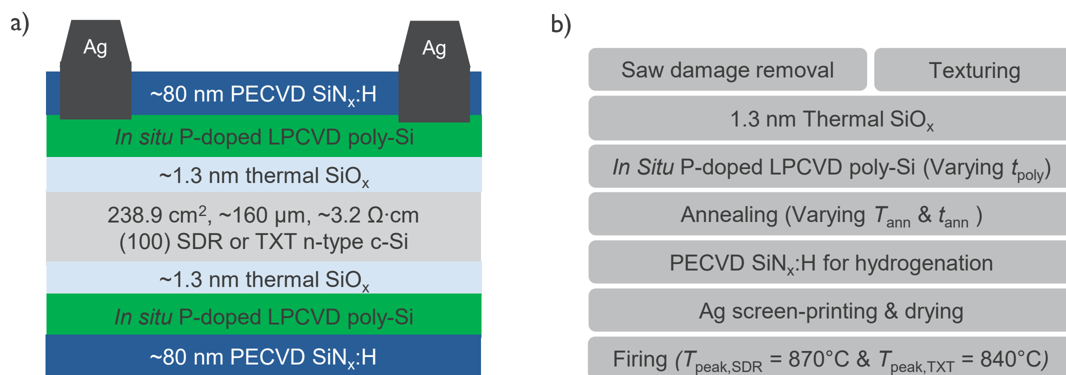

Figure 2. a) Design of the symmetrically passivated samples. b) Process flow followed for fabricating the samples in a).

Two experimental splits were introduced while preparing the samples. The first split was made at the LPCVD step, by varying the deposition duration for growing films that are 100 nm, 150 nm, and 200 nm thick. This screening of t_{poly} was performed only for the TXT samples and for a single annealing condition at a temperature (T_{ann}) of 900°C for a duration (t_{ann}) of 60 min.

The second experimental split was regarding the post-LPCVD annealing process: T_{ann} of 800°C or 900°C, and t_{ann} of 30 min or 60 min were chosen. For this split, t_{poly} was fixed at 150 nm.

The screen-printed Ag finger grid included regions with varying metallization fraction (*MF*) and non-metallized regions, designed to allow a full characterization of the passivating contacts (see Fig. S1a) in Supplementary Information). At the non-metallized regions, minority carrier lifetime (τ) measurements were performed. The resulting injection level (Δn) dependent lifetime data were used for extracting the J_0 of the poly-Si passivating contact in passivated regions ($J_{0,p}$) at $\Delta n = 10^{16}$ cm^{-3}, as well as τ at $\Delta n = 10^{15}$ cm^{-3}, the implied open circuit voltage (iV_{oc}), and the implied fill factor (*iFF*). Furthermore, J_0 of the passivating contact in metallized regions ($J_{0,m}$) was determined by using the lifetime data together with photoluminescence (PL) images of all regions with varying *MF*, following the method in (Comparotto et al., 2017).

The same samples were also used for measuring the ρ_c of the poly-Si passivating contacts by transfer length method (TLM) measurements. It is important to note that the original TLM measurements yielded the ρ_c between the Ag fingers and the poly-Si ($\rho_{c,m}$). To determine the ρ_c across the total Ag/poly-Si/SiO_x/c-Si stack, which is denoted $\rho_{c,t}$ and accounts for the contribution of the carrier transport through the SiO_x layer unlike $\rho_{c,m}$, TLM measurements were repeated after introducing dicing saw cuts at both sides of each Ag finger (see Fig. S1b) and S1c) in Supporting Information).

2.4 Optical Impact of the Poly-Si Passivating Contacts

The final investigation in this work focused on the optical losses due to parasitic absorption in the poly-Si films when applied at the rear side of Si solar cells. For this purpose, non-metallized solar cell precursors were prepared with boron-diffused front emitter and poly-Si passivating contacts at the rear. A detailed description of the design and fabrication of samples of this type is available elsewhere (Fırat et al., 2019). In this work, two sets of samples were prepared for studying the impact of (i) t_{poly} and (ii) the $N_{D,act}$ level on the resulting optical losses, which are mainly due to FCA. For the first set, the poly-Si films were deposited using T_{dep} = 590°C, Q_H = 10 slm, and Q_P = 200 sccm, with varying t_{poly} of 100 nm, 150 nm, and 200 nm. For the second set, t_{poly} was selected as 150 nm, while the LPCVD parameters were T_{dep} = 590°C, Q_H = 10 slm, and a varying Q_P of 20 sccm, 50 sccm, and 200 sccm. The variation of Q_P allowed

determining the impact of the $N_{D,act}$ level in the poly-Si, which depends on Q_P. All samples of this study underwent a post-LPCVD anneal at 900°C for 60 min.

The samples were characterized by reflectance measurements. A short circuit current density (J_{sc}) value was determined for each sample by PC1D simulations, based on the measured reflectance data. The optical losses due to the poly-Si films (ΔJ_{sc}) were then determined by comparing the simulated J_{sc} of the samples with poly-Si passivating contacts to the simulated J_{sc} of reference samples with no poly-Si but $POCl_3$-diffused back surface fields (BSF) instead. A detailed description of the data analysis and simulation method used can be found in the literature (Fırat et al., 2019).

3 Results and Discussion

3.1 Development of *In Situ* P-Doped LPCVD Poly-Si Films

The baseline process introduced in Table 1 was used in our previous work and yielded a low $N_{D,act}$ of $2.6 \cdot 10^{19}$ cm^{-3}, resulting in a poor-quality passivating contact (Fırat et al., 2019). This work aimed at improving this process to obtain films with $N_{D,act}$ over $1 \cdot 10^{20}$ cm^{-3} to enable the fabrication of excellent passivating contacts, while also limiting the drop in r_{dep} compared to the deposition of intrinsic poly-Si to a minimum, to ensure a high process throughput.

The findings regarding the impact of varying T_{dep} on $N_{D,act}$ and r_{dep} of the poly-Si films are depicted in Fig. 3a). These lead to two conclusions: decreasing T_{dep} from 720 °C to 590 °C (i) yields an increase in $N_{D,act}$ of ~3 times, and (ii) reduces r_{dep} exponentially. The latter observation is well-known and shows that, for the range of T_{dep} values used, the deposition is limited by the reaction rate of the decomposition of SiH_4, which increases exponentially with T_{dep} (Learn and Foster, 1987). The activation energy of this deposition process was extracted as 1.65 eV and is in agreement with the literature (Kamins, 1998). The increase in $N_{D,act}$ with decreasing T_{dep} is attributed to reduced PH_3 desorption during poly-Si growth (Learn and Foster, 1987).

The impact of T_{dep} on the structure of the poly-Si films can be qualitatively understood using Raman spectroscopy, as shown in Fig. 3b), where the spectra are normalized to the same maximum intensity. Even though only a few spectra are depicted for clarity purposes, the following discussion is valid for all T_{dep} studied. While a peak at a Raman shift of 521 cm^{-1}

was detected for all samples indicating polycrystalline content, a significantly elevated baseline was found for $T_{dep} \leq 570$ °C, showing the partly amorphous structure of the corresponding films (Iqbal and Veprek, 2000). For T_{dep} of 590°C and above, the films are fully crystalline, but a surprising side-peak was found at a Raman shift close to 500 cm^{-1}. This peak is attributed to scattering at grain boundaries inside the poly-Si film (Gao and Yin, 2017), the strength of which indicates an abundance of grain boundaries and thus a small grain size. The grain size could not be measured directly in this work, as TEM images of the developed poly-Si films indicated grains of irregular shapes and sizes. Instead, XRD measurements were performed to determine the average crystallite size, which is a lower bound and an indicator for the average grain size, allowing for sample-to-sample comparison (Joubert et al., 1987). For the poly-Si films grown at varying T_{dep}, the crystallite size by XRD was found to be between 15 and 24 nm, which, surprisingly, did not seem to be a function of T_{dep}. In accordance with the small crystallite size, $\mu_{H,n}$ by Hall measurements is also quite low, between 3.3 and 9.4 cm^2/Vs. Interestingly, unlike the crystallite size, $\mu_{H,n}$ was found to depend systematically on, in particular, increase with, T_{dep}. This is attributed to reduced impurity scattering due to the significant decrease in $N_{D,act}$ with increasing T_{dep}, because in poly-Si, impurity scattering is known to limit $\mu_{H,n}$ for $N_{D,act} > 10^{18}$ cm^{-3}, which is the case for the films studied in this work (Kamins, 1971; Mandurah et al., 1979).

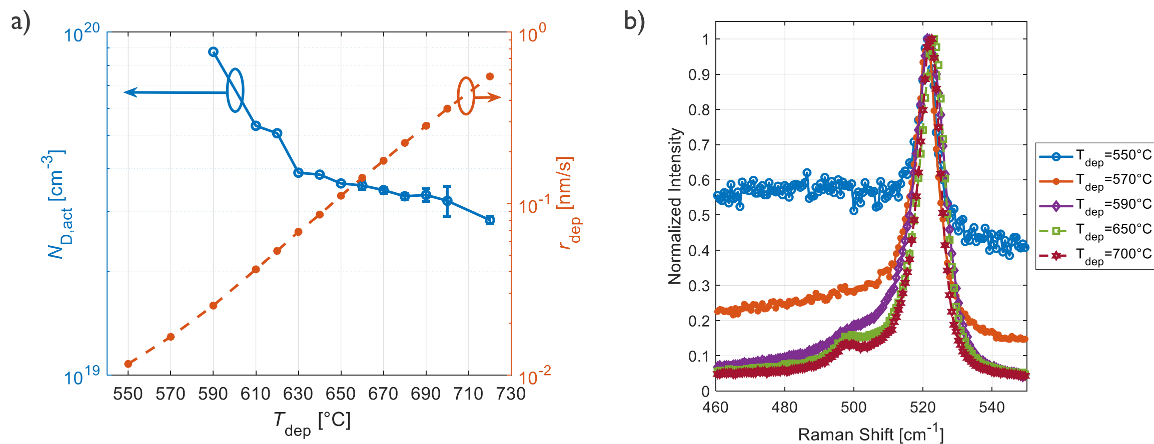

Figure 3. a) Active dopant concentration ($N_{D,act}$) in the poly-Si films and the poly-Si deposition rate (r_{dep}) as a function of the deposition temperature (T_{dep}). b) Raman spectra of poly-Si films normalized to the same maximum intensity, deposited at various T_{dep}.

Next, the impact of reducing Q_H was studied and it was found in Fig. 4a) that lower Q_H leads to a higher $N_{D,act}$, while N_D increases only marginally, which indicates enhanced dopant activation. Moreover, a lower Q_H also yields a higher r_{dep} by ~40-50% as depicted in Fig. 4b). These increases are attributed to two types of impact of Q_H on the *in situ* doped film deposition.

First, lowering Q_H reduces the dilution of the precursors PH_3 and SiH_4, which might increase the rate with which P and Si atoms are incorporated into the poly-Si film. Second, H_2 is a product of the decomposition reactions of PH_3 and SiH_4, which are thus accelerated by lowering Q_H (Kamins, 1998). Structurally, reduction in Q_H does not yield significant changes as found by Raman spectroscopy and XRD measurements; the films were polycrystalline with crystallite sizes of 16-22 nm. Based on these findings, the lowest Q_H which could be reliably controlled in the deposition tool, equal to 10 slm, was selected for further development. Moreover, the difference between $N_{D,act}$ and N_D in Fig. 4a) shows that only ~15-25% of the P atoms in the poly-Si were electrically active, which implies that the Q_P of 500 sccm used in this study so far was too high, suggesting a reduction in Q_P.

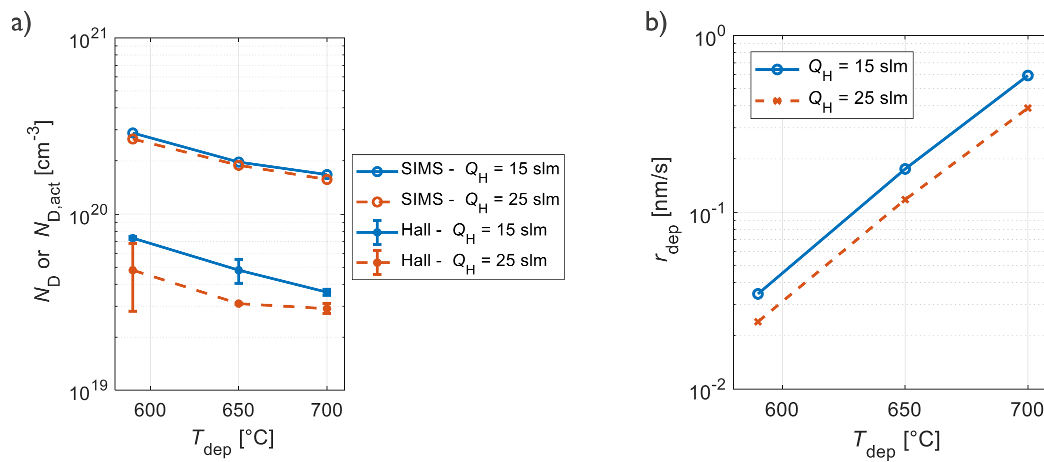

Figure 4. a) Total (N_D) and active ($N_{D,act}$) dopant concentration in poly-Si films as determined by SIMS and Hall measurements, respectively, as a function of the deposition temperature (T_{dep}) for two different H_2 flows of 15 and 25 slm. b) The corresponding poly-Si deposition rates.

According to the findings in Fig. 3 and Fig. 4, T_{dep} = 590 °C and Q_H = 10 slm were selected for further film development, in order to achieve a high $N_{D,act}$ while limiting the drop in r_{dep}. For these parameters, screening lower Q_P as suggested above led to the results in Fig. 5. From the $N_{D,act}$ values in Fig. 5a), it is evident that a maximum exists at a Q_P of approximately 200 sccm, beyond which, interestingly, $N_{D,act}$ decreases. While a similar decrease in N_D was measured by SIMS beyond a Q_P of 250 sccm and might partly explain the reduction in $N_{D,act}$, another reason might be the decrease in the poly-Si grain size with increasing Q_P, indicated by the TEM images of the samples with Q_P = 0 and 50 sccm, which are depicted in Fig. 5b) and c), respectively. These images show that (i) significantly larger grains with sizes up to 100 nm and beyond are observed in Fig. 5b) for Q_P = 0 than in Fig. 5c) for Q_P = 50 sccm, and (ii) the grains are of irregular size, leading to difficulties in quantitatively determining a precise grain size value.

Therefore, the crystallite size determined by XRD was also investigated as a more quantitative measure, which follows a decreasing trend with increasing Q_P as shown in Fig. 5d). We would like to note that the trend in crystallite size has an irregularity at Q_P = 150 sccm. This irregularity is not well-understood but could be due to a process drift, as samples with $Q_P <$ 150 sccm and $Q_P \geq$ 150 sccm were processed in two different experimental runs. Thus, overall, the observed behavior of the crystallite size in Fig. 5d) further corroborates the reduction in the grain size with increasing Q_P. Such lower grain size probably led to the segregation of a higher portion of P to the grain boundaries, where P is known to be electrically inactive (Kamins, 1998). Hence, enhanced grain boundary segregation of P together with the saturating or decreasing trend of N_D might have reduced $N_{D,act}$ beyond a Q_P of 200 sccm, explaining the data in Fig. 5a).

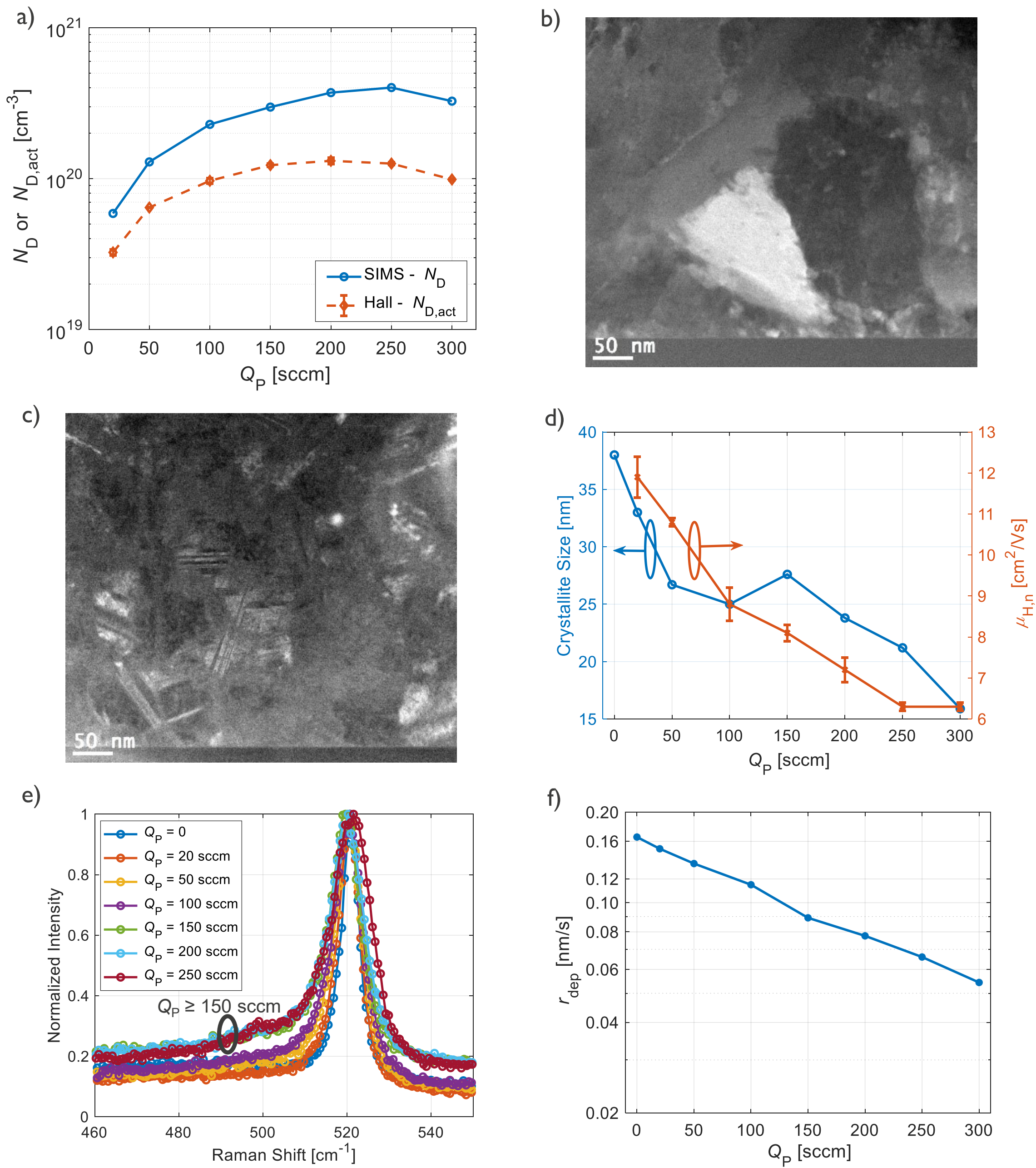

Figure 5. a) Total (N_D) and active ($N_{D,act}$) dopant concentration as determined by SIMS and Hall measurements, respectively, as a function of the PH_3 flow (Q_P), in poly-Si films deposited at 590°C with a H_2 flow of 10 slm. b) TEM image of the poly-Si film deposited with Q_P = 0. c) TEM image of the poly-Si film deposited with Q_P = 50 sccm. d) Crystallite size from XRD and electron Hall mobility ($\mu_{H,n}$) of the poly-Si films as a function of Q_P. e) Raman spectra of the poly-Si films normalized to the same maximum intensity, for various Q_P. f) Poly-Si deposition rate (r_{dep}) as a function of Q_P.

The reduction in the grain size with increasing Q_P also explains the corresponding decrease in $\mu_{H,n}$, depicted in Fig. 5d), since poly-Si films with smaller grains would have more grain boundaries acting as barriers to electrical transport. The impact of the reduction in the grain size is also observed in the Raman spectra in Fig. 5e), where the side peak at a Raman shift of ~500 cm^{-1}, which is attributed to a smaller grain size, starts to appear for $Q_P \geq 150$ sccm. The

Raman spectra also show an elevated baseline signal particularly for $Q_P \geq 150$ sccm, which indicates an increasing amorphous content in the deposited films.

Most importantly, Fig. 5 shows that an $N_{D,act} > 1 \cdot 10^{20}$ cm^{-3}, which is considered necessary for the fabrication of high-quality passivating contacts, can be achieved in the *in situ* P-doped poly-Si films by LPCVD, for T_{dep} = 590 °C, Q_H = 10 slm, and Q_P between 100 and 300 sccm. Interestingly, reducing Q_P from its baseline process value of 500 sccm was necessary to achieve such high $N_{D,act}$. Such reduction is also beneficial in terms of the deposition process throughput, as Fig. 5f) shows an increase in r_{dep} for decreasing Q_P, which is due to the presence of fewer PH_3 molecules blocking adsorption sites for SiH_4 during the film growth (Kamins, 1998; Meyerson and Yu, 1984; Mulder et al., 1990). For further development in this work, Q_P was selected as 200 sccm, as this leads to the maximum $N_{D,act}$ value of $1.3 \cdot 10^{20}$ cm^{-3}. The corresponding r_{dep} is 0.078 nm/s, which increases the duration to deposit a typical 150 nm thick poly-Si film to ~32 min, which is only ~17 min longer than the case of Q_P = 0 i.e., intrinsic poly-Si deposition. Thus, this result demonstrates that fabrication of *in situ* doped poly-Si films can be less time-consuming than *ex situ* doped films because the extra doping step would lead to an overall longer process despite the shorter LPCVD step. Moreover, r_{dep} of the *in situ* doped films can be further boosted by up to 50% without a significant loss in $N_{D,act}$ by exploring the Q_P range of 100-200 sccm, as Fig. 5a) and 5f) indicate. It is important to note that the limited r_{dep} drop was demonstrated with a single-wafer tool here; nevertheless, it is expected that processes achieving similar r_{dep} can also be developed with industrial equipment.

3.2 Impact of Annealing on the *In Situ* P-Doped LPCVD Poly-Si Films

Annealing of *in situ* doped poly-Si films is generally considered necessary for increased activation of dopants and for obtaining low J_0 and ρ_c values for the passivating contact (Yan et al., 2021). However, since a high $N_{D,act}$ in the poly-Si films was achieved in this work without annealing, the initial efforts of incorporating these films in passivating contacts included a process design without annealing (Fırat et al., 2020). While an excellent passivation quality with $J_{0,p} < 5$ fA/cm^2 was obtained using such non-annealed films, the $\rho_{c,m}$ values remained above 37.6 mΩ·cm^2 and were thus too high for application in high-efficiency bifacial Si solar cells, for which our target value is below 5 mΩ·cm^2. Thus, the impact of post-LPCVD annealing on the *in situ* doped poly-Si films was studied in this work.

Initial findings for passivating contacts annealed in the airtight LPCVD equipment in H_2 ambient at p = 40 Torr, however, also indicated high $\rho_{c,m}$ values, which surprisingly increased with increasing annealing thermal budget (Fırat et al., 2020). This was attributed to loss of dopants to the ambient during annealing, which is verified in this work by means of SIMS measurements, as shown in Fig. 6a). Both the overall reduction in N_D and the gradual drop towards the surface are clear signs of loss of P to the ambient. In addition, Hall measurements showed that $N_{D,act}$ drops as well, for T_{ann} = 800°C, to $5.7 \cdot 10^{19}$ cm^{-3}. For T_{ann} = 900°C, the poly-Si film was too resistive, and no Hall measurement could be performed.

The reason behind the dopant loss is identified as the lack of oxide formation at the surface of the poly-Si film during annealing in the airtight LPCVD equipment, as the presence of a surface oxide layer is necessary for containing the dopants in the poly-Si according to the literature (Murarka, 1984). The low pressure of the annealing ambient is excluded as cause for the dopant loss, since annealing in the same airtight equipment at atmospheric pressure still led to a similar P loss (data not shown here). By performing the annealing in an equipment which is not airtight and ensuring that, during the process, the poly-Si film surface is covered by an oxide, successful mitigation of the dopant loss is demonstrated as shown in Fig. 6a). This leads to a flat profile of N_D across the entire poly-Si film with only a slight drop compared to N_D before annealing, both in O_2 and N_2 ambient. Both anneals also yield a slight increase in $N_{D,act}$ from $1.3 \cdot 10^{20}$ cm^{-3} to $1.5 \cdot 10^{20}$ cm^{-3}, which is attributed to further dopant activation. As annealing in O_2 ambient partly consumes the poly-Si film due to oxidation, annealing in N_2 ambient, combined with pre-coating poly-Si with a wet-chemical SiO_x layer, is preferred for the rest of this work.

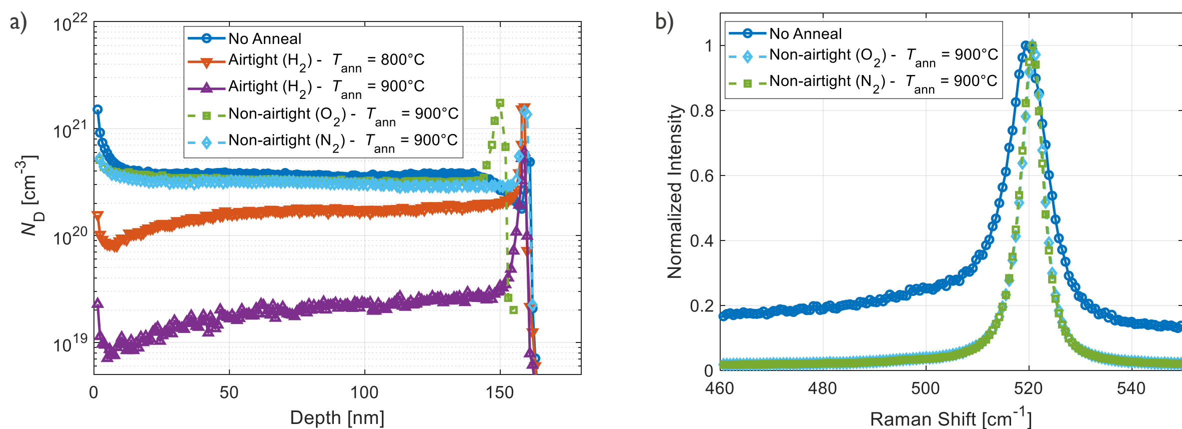

Figure 6. a) Total dopant concentration (N_D) in poly-Si films after various annealing procedures, as determined by SIMS measurements. b) Raman spectra of the poly-Si films before and after annealing.

Annealing without dopant loss was found to modify the poly-Si films structurally as well. Raman spectra in Fig. 6b) show that the baseline signal due to the amorphous content of the film fully disappears after annealing, indicating full crystallization. Moreover, annealing probably led to grain growth, indicated by an increase in the crystallite size of poly-Si films from 30 nm to 35 nm. As expected, these structural changes boosted $\mu_{H,n}$, which more than tripled from 7.8 cm^2/Vs to 28.4 cm^2/Vs.

Given its benefits, the post-LPCVD annealing process without dopant loss was used for the passivating contact development in this work. Further development of annealing-free single-step fabrication of *in situ* doped passivating contacts was identified as a target of future work.

3.3 Integration of the Developed *In Situ* P-Doped LPCVD Poly-Si Films in Passivating Contact Structures

The developed *in situ* doped poly-Si films were combined with thermally grown interfacial SiO_x films and treated with the developed post-LPCVD annealing process for the realization of passivating contacts. The choice of thermal oxidation for the fabrication of the SiO_x layer was made based on the findings of our initial experiments comparing oxides grown by various techniques, which showed the superior performance of thermal SiO_x (Fırat et al., 2020).

The performance of the resulting passivating contacts is summarized in Fig. 7 and Fig. 8. Comparison of different annealing thermal budgets in Fig. 7 shows that a T_{ann} of 900°C is superior to 800°C for obtaining an excellent passivation quality, as this cut both $J_{0,p}$ and $J_{0,m}$ approximately by half (see Fig. 7a)). Moreover, a T_{ann} of 900°C is necessary for obtaining a sufficiently low $\rho_{c,m} < 5$ $m\Omega \cdot cm^2$ (see Fig. 7b)). Furthermore, when performing $\rho_{c,t}$ measurements, T_{ann} = 800°C led to non-Ohmic contacts for which no $\rho_{c,t}$ value could be extracted. This not only illustrates further the need for post-LPCVD annealing as discussed in Section 3.2, but also shows that T_{ann} must be high enough, for example 900°C, for facilitating proper carrier transport through the SiO_x layer. For T_{ann} = 900°C, in contrast to T_{ann} = 800°C, Ohmic contacts with $\rho_{c,t}$ of 20.1-66.9 $m\Omega \cdot cm^2$ were obtained. While these $\rho_{c,t}$ values are quite high compared to $\rho_{c,m}$, they are acceptable for application of these passivating contacts at the rear side of bifacial Si solar cells, where a blanket poly-Si layer is normally used. This is because $\rho_{c,t}$ is associated with a full-area contact and thus needs to fulfill less stringent requirements than $\rho_{c,m}$, which applies to the significantly smaller contact area between Ag

fingers and the poly-Si film. In addition to T_{ann}, increasing t_{ann} from 30 min to 60 min was also found to be beneficial, albeit less critical, for reducing $J_{0,p}$, $J_{0,m}$, and $\rho_{c,m}$. Interestingly, a similar impact on $\rho_{c,t}$ could only be found for the case with an SDR surface.

The positive impact of higher T_{ann} and t_{ann} on the performance of poly-Si passivating contacts is attributed to three factors. First, $N_{D,act}$ in the poly-Si film increases slightly upon annealing as shown in Section 3.2. Second, annealing, particularly for higher thermal budgets, enhances the diffusion of P from the poly-Si into the c-Si substrate as known from the literature (Kamins, 1998). These lead to a reduced minority carrier concentration at the interface between the passivating contact and the c-Si substrate and thus decrease $J_{0,p}$ and $J_{0,m}$. Furthermore, higher $N_{D,act}$ in the poly-Si reduces $\rho_{c,m}$, while higher doping at both sides of the interfacial SiO_x layer yields favorable band bending, which enhances tunneling through SiO_x and reduces $\rho_{c,t}$ (Steinkemper et al., 2015). Lastly, the interfacial SiO_x film undergoes structural reconstruction during annealing. This leads both to a reduction in the interface defect density at the c-Si/SiO_x interface, which suppresses recombination of minority carriers and thus $J_{0,p}$ and $J_{0,m}$, and to formation of pinholes or nanopits in the SiO_x film, which facilitates the transport of majority carriers and thus reduces $\rho_{c,t}$ (Galleni et al., 2021; Liu et al., 2019). Despite these benefits of annealing, it is important to note that extreme thermal budgets can degrade passivation during annealing by yielding a pinhole density in the interfacial SiO_x that is too high and diffusion of P into the Si bulk that is too excessive, which is the reason for not considering higher T_{ann} in this work.

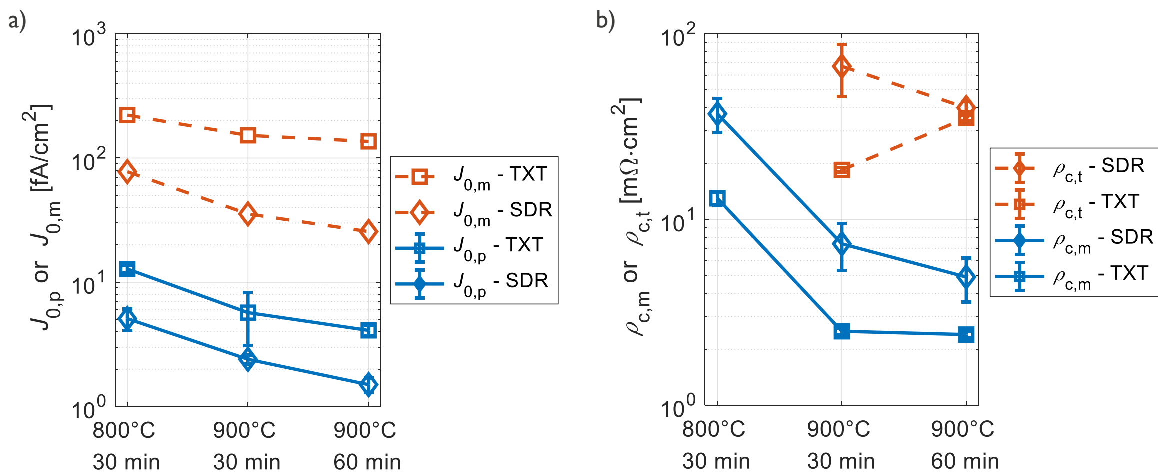

Figure 7. Impact of annealing temperature and duration on poly-Si passivating contacts in terms of: a) recombination current density in passivated ($J_{0,p}$) and in Ag screen-printed ($J_{0,m}$) regions, and b) contact resistivity of screen-printed fingers to the poly-Si ($\rho_{c,m}$) and of the total passivating contact stack of Ag/poly-Si/SiO_x/c-Si ($\rho_{c,t}$), obtained on saw-damage removed (SDR) and textured (TXT) wafers.

In addition to the impact of annealing, Fig. 7 shows that the rougher surface morphology of TXT wafers leads to higher $J_{0,p}$ and $J_{0,m}$, but lower $\rho_{c,m}$ and $\rho_{c,t}$, compared to SDR wafers. This is expected given that the surface area of TXT wafers is larger than that of SDR wafers by a factor of ~1.7. However, the measured values differ mostly by a factor of 2 to 3, which means that the differences cannot be fully explained by the increased surface area of TXT wafers. While further study is needed to determine the additional reasons, potentially poorer thickness homogeneity and integrity of the interfacial SiO_x layer on rougher TXT surfaces can be speculated as possible causes for this.

Despite the differences, it is evident from Fig. 7 that excellent passivating contacts can be obtained both on SDR and TXT surfaces with the *in situ* P-doped poly-Si films developed in this work. Upon annealing at 900°C for 60 min, $J_{0,p} < 5$ fA/cm^2 and $\rho_{c,m} < 5$ mΩ·cm^2 are achieved simultaneously, on both surfaces. Moreover, Fig. 8 shows that the passivating contacts can be further improved by increasing t_{poly} for the case of TXT samples, which is expected to be applicable for SDR surfaces as well. First, it is evident from Fig. 8a) that $J_{0,m}$ can be decreased by about an order of magnitude by increasing t_{poly} from 100 nm to 200 nm. This suggests that thicker poly-Si films are better in preventing damage from aggressive screen-printed metallization, which might occur due to local Ag spiking through the passivating contact during the fire-through process (Çiftpinar et al., 2017). In addition to $J_{0,m}$, thicker poly-Si layers seem to also yield slightly lower $J_{0,p}$ and $\rho_{c,m}$, as shown in Fig. 8a) and 8b), respectively. Furthermore, $\rho_{c,t}$ was found to increase with increasing t_{poly} (see Fig. 8b)). The reasons behind the findings regarding $J_{0,p}$, $\rho_{c,m}$, and $\rho_{c,t}$ are not well-understood.

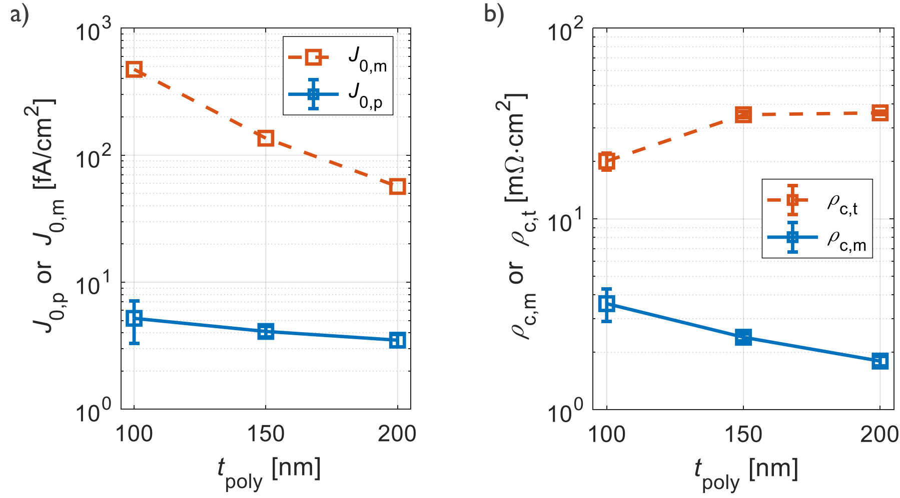

Figure 8. Impact of the poly-Si film thickness (t_{poly}) on poly-Si passivating contacts in terms of: a) recombination current density in passivated ($J_{0,p}$) and in Ag screen-printed ($J_{0,m}$) regions, and b) contact resistivity of screen-printed fingers to the poly-Si ($\rho_{c,m}$) and of the total passivating contact stack of Ag/poly-Si/SiO_x/c-Si ($\rho_{c,t}$), obtained on textured (TXT) wafers.

Concluding the poly-Si passivating contact development, the figures of merit characterizing the best passivating contacts obtained on SDR and TXT surfaces are summarized in Table 2. These show that, apart from the excellent J_0 and ρ_c parameters, the developed passivating contacts enable outstanding $\tau > 7$ ms, $iFF > 86\%$ and $iV_{oc} > 740$ mV on both surfaces. It is important to note that the results in Table 2 are on par with the data reported in the literature for typical high-quality passivating contacts with poly-Si films fabricated by the standard industrial process combining LPCVD and *ex situ* doping (J_0 = 1-4 fA/cm^2 and ρ_c = 0.5-5 mΩ·cm^2) (Çiftpinar et al., 2017; Padhamnath et al., 2020; Yan et al., 2021). Hence, the findings presented in this paper clearly show the promise of combining the LPCVD technique with *in situ* P-doping for fabricating poly-Si films for contact passivation of Si solar cells. To demonstrate the full potential of this process, integration of the developed passivating contacts in industrially processed solar cells is planned as future work.

Table 2. Summary of all figures of merit of the best passivating contacts obtained on SDR and TXT surfaces, for poly-Si film thicknesses of 150 nm and 200 nm, respectively.

Surface	t_{poly} **[nm]**	τ **[ms]**	***iFF*** **[%]**	iV_{oc} **[mV]**	$J_{0,p}$ **[fA/cm^2]**	$J_{0,m}$ **[fA/cm^2]**	$\rho_{c,m}$ **[mΩ·cm^2]**	$\rho_{c,t}$ **[mΩ·cm^2]**
SDR	150	9.4±1.9	86.5±0.3	747.2±0.2	1.5±0.2	25.6	4.9±1.3	40.0±3.3
TXT	200	7.2±0.1	86.0±0.1	740.9±0.4	3.5±0.4	56.7	1.8±0.1	36.0±0.7

3.4 Optical Impact of the Poly-Si Passivating Contacts

While poly-Si passivating contacts offer excellent electrical properties as shown in Section 3.3, it is important to also consider and characterize the optical losses caused by parasitic absorption in the highly doped poly-Si film of the contacts. As poly-Si passivating contacts are mostly used at the rear side of Si solar cells, optical losses arising from such application are studied here.

The J_{sc} losses (ΔJ_{sc}) due to increasing t_{poly} are depicted in Fig. 9a). As expected, thicker poly-Si films lead to higher ΔJ_{sc} due to increased parasitic FCA in the heavily doped poly-Si films. In the t_{poly} range studied, the increase in ΔJ_{sc} seems to be linear, and applying a linear fit to the data reveals a ΔJ_{sc} of 0.41 mA/cm^2 per 100 nm increase in t_{poly}, for $N_{D,act} = 1.5 \cdot 10^{20}$ cm^{-3}, which is in reasonable agreement with our previous work (Fırat et al., 2019). This result shows that a trade-off exists between ΔJ_{sc} and the electrical figures of merit in Fig. 8, among which $J_{0,m}$ decreases strongly with increasing t_{poly}. Hence, t_{poly} may not be increased arbitrarily to improve the passivating contact electrically, but it needs to be optimized considering the associated optical losses as well.

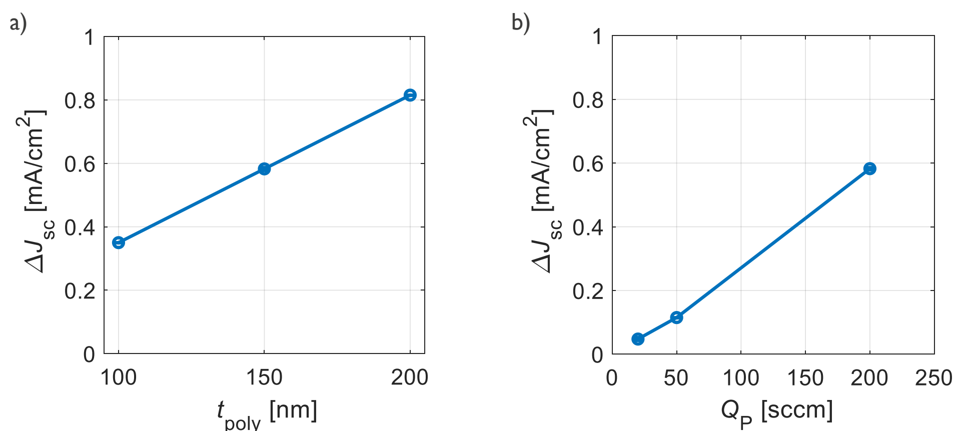

Figure 9. Simulated optical losses due to poly-Si films at the rear side of Si solar cell structures in terms of short circuit current density (ΔJ_{sc}) as a function of a) poly-Si thickness (t_{poly}) for a PH_3 flow of 200 sccm and of b) PH_3 flow (Q_P) for a t_{poly} of 150 nm.

For a given t_{poly}, the FCA and the corresponding ΔJ_{sc} are expected to depend on $N_{D,act}$, which can be altered by varying Q_P as shown in Fig. 5a). This is demonstrated here, as the findings in Fig. 9b) show that a Q_P of 50 sccm or below, which reduces $N_{D,act}$ below $1 \cdot 10^{20}$ cm^{-3}, limits ΔJ_{sc} to ~0.1 mA/cm^2 and below. Hence, thicker poly-Si films yielding lower $J_{0,m}$ could be optically tolerated for such reduced $N_{D,act}$. Furthermore, reducing Q_P would yield the additional

benefit of an increased r_{dep} (see Fig. 5f)) and thus process throughput. Given these potential advantages, the feasibility of fabricating passivating contacts with a lower $N_{D,act}$ level was assessed by fabricating a test sample with a Q_P of 50 sccm and a T_{ann} of 900°C. While the resulting passivating contact delivered excellent passivation with $J_{0,p} < 5$ fA/cm^2, $\rho_{c,m}$ was found to be greater than 50 mΩ·cm^2, which is too high for use in typical bifacial Si solar cells. Nevertheless, exploring the Q_P range of 50-200 sccm might yield sufficiently low $\rho_{c,m}$ while still allowing a reduction in ΔJ_{sc} as well as an increase in r_{dep}. Such optimization of Q_P towards lower values may also be assisted by improving screen-printing pastes for poly-Si passivating contacts, which might enable low $\rho_{c,m}$ for $N_{D,act}$ below $1 \cdot 10^{20}$ cm^{-3}.

4 Summary and Outlook

For the fabrication of heavily P-doped poly-Si films for contact passivation of Si solar cells, the PV industry mainly relies on the high-throughput LPCVD technique combined with *ex situ* doping methods. As this is an inherently two-step process and prolongs the fabrication, a leaner approach is targeted in this work, which relies on *in situ* P-doped LPCVD-based poly-Si films. When developing the *in situ* doped films, particular attention was paid to the challenge of obtaining a high $N_{D,act}$ while keeping the drop in r_{dep} due to the introduction of the dopant precursor to a minimum. By means of a systematic investigation of the impact of the LPCVD parameters T_{dep}, Q_H, and Q_P on electrical and structural properties of the poly-Si films, a high $N_{D,act}$ of $1.3 \cdot 10^{20}$ cm^{-3} was obtained for $T_{dep} = 590$ °C, $Q_H = 10$ slm, and $Q_P = 200$ sccm. This was achieved with a limited drop in r_{dep}, with the resulting r_{dep} being 0.078 nm/s. Impact of post-LPCVD annealing on these films was also studied, which resulted in the development of an annealing process that further crystallizes the films, yielding a slight increase in $N_{D,act}$ to $1.5 \cdot 10^{20}$ cm^{-3} and a $\mu_{H,n}$ of 28.4 cm^2/Vs.

The developed poly-Si films were also incorporated in poly-Si passivating contacts, the performance of which was assessed both on SDR and TXT surfaces for varying annealing thermal budget and t_{poly}. Among the parameter range explored for annealing, increasing both T_{ann} and t_{ann} was found to provide lower J_0 and ρ_c values, and thus to be beneficial for the passivating contact performance. Similarly, increasing t_{poly} also enhanced the passivation quality obtainable, particularly in form of a reduced $J_{0,m}$. By using the optimum annealing condition with $T_{ann} = 900$°C and $t_{ann} = 60$ min, excellent passivating contacts with $J_{0,p} < 5$ fA/cm^2 and $\rho_{c,m} < 5$ mΩ·cm^2 were demonstrated on both SDR and TXT surfaces. Parasitic absorption losses caused by the developed passivating contacts were also investigated,

predicting a J_{sc} loss of 0.41 mA/cm^2 per a 100 nm increase in t_{poly}, when using the contacts at the rear side of Si solar cells.

The findings of this work will be followed up by integrating the developed passivating contacts in Si solar cells, to demonstrate their potential in terms of the high efficiencies they can enable. Moreover, further optimization of the *in situ* doping process during LPCVD will be undertaken to increase r_{dep} and decrease J_{sc} losses while preserving the excellent passivating contact properties by exploring slightly higher T_{dep} and slightly lower Q_P values. Lastly, an effort will be made to develop passivating contacts using *in situ* doped LPCVD-based poly-Si films fabricated by a simple single-step process, i.e., by a process which does not involve a post-LPCVD anneal.

Acknowledgments

The authors would like to acknowledge Rajiv Sharma from KU Leuven for his help with the interfacial oxide development, Sukhvinder Singh and Patrick Choulat from Imec for their help with the contact resistivity measurements and sample fabrication, Thomas Nuytten and Stefanie Sergeant from Imec for the Raman spectroscopy measurements, Bastien Douhard and Mustafa Ayyad from Imec for SIMS measurements, Maxim Korytov, Laura Nelissen, and Patricia van Marcke from Imec for the TEM specimen preparation and measurements, and Janusz Bogdanowicz from Imec for his help with the analysis of the Hall measurement data.

This work was supported by the European Union’s Horizon2020 Programme for research, technological development, and demonstration [grant number 857793]; and by the Kuwait Foundation for the Advancement of Sciences [grant number CN18-15EE-01].

References

Ahmed, W., Ahmed, E., 1992. An Investigation of LPCVD and PECVD of in situ Doped Polycrystalline Silicon for VLSI. Adv. Mater. Opt. Electron. 1, 255–259. https://doi.org/10.1002/amo.860010508

Chen, R., Zheng, P., Wright, M., Chen, D., Yang, J., Ciesla, A., Wenham, S., 2021. 24.58% efficient commercial n-type silicon solar cells with hydrogenation. Prog. Photovoltaics Res. Appl. 1–6. https://doi.org/10.1002/pip.3464

Chen, Y., Chen, D., Liu, C., Wang, Z., Zou, Y., He, Y., Wang, Y., Yuan, L., Gong, J., Lin, W., Zhang, X., Yang, Y., Shen, H., Feng, Z., Altermatt, P.P., Verlinden, P.J., 2019.

Mass production of industrial tunnel oxide passivated contacts (i-TOPCon) silicon solar cells with average efficiency over 23% and modules over 345 W. Prog. Photovoltaics Res. Appl. 27, 827–834. https://doi.org/10.1002/pip.3180

Çiftpinar, H.E., Stodolny, M.K., Wu, Y., Janssen, G.J.M., Löffler, J., Schmitz, J., Lenes, M., Luchies, J.M., Geerligs, L.J., 2017. Study of screen printed metallization for polysilicon based passivating contacts, in: Energy Procedia. Elsevier Ltd, pp. 851–861. https://doi.org/10.1016/j.egypro.2017.09.242

Comparotto, C., Theobald, J., Lossen, J., Mihailetchi, V.D., 2017. Understanding Contact Formation on n-PERT-RJ Solar Cells, in: 33rd European Photovoltaic Solar Energy Conference and Exhibition. pp. 832–836. https://doi.org/10.4229/EUPVSEC20172017-2CV.2.23

Feldmann, F., Mack, S., Steinhauser, B., Tutsch, L., Polzin, J.-I., Temmler, J., Moldovan, A., Wolf, A., Rentsch, J., Hermle, M., Glunz, S.W., 2018. Towards industrial manufacturing of TOPCon. Photovoltaics Int. 40, 46–55.

Fischer, M., Woodhouse, M., Herritsch, S., Trube, J., 2021. International Technology Roadmap for Photovoltaic 2020 Results.

Fırat, M., Payo, M.R., Duerinckx, F., Luchies, J.M., Lenes, M., Poortmans, J., 2019. Characterization of absorption losses in rear side N-type polycrystalline silicon passivating contacts. AIP Conf. Proc. 2147. https://doi.org/10.1063/1.5123831

Fırat, M., Radhakrishnan, H.S., Payo, M.R., Duerinckx, F., Sharma, R., Poortmans, J., 2020. In Situ Phosphorus-Doped Poly-Si by Low Pressure Chemical Vapor Deposition for Passivating Contacts, in: Conference Record of the IEEE Photovoltaic Specialists Conference. pp. 0160–0163. https://doi.org/10.1109/PVSC45281.2020.9300543

Galleni, L., Fırat, M., Radhakrishnan, H.S., Duerinckx, F., Tous, L., Poortmans, J., 2021. Mechanisms of charge carrier transport in polycrystalline silicon passivating contacts. Sol. Energy Mater. Sol. Cells 232, 111359. https://doi.org/10.1016/j.solmat.2021.111359

Gao, Y., Yin, P., 2017. Origin of asymmetric broadening of Raman peak profiles in Si nanocrystals. Sci. Rep. 7. https://doi.org/10.1038/srep43602

Grahn, J. V., Pejnefors, J., Sandén, M., Zhang, S. -L., Östling, M., 1997. Characterization of In Situ Phosphorus-Doped Polycrystalline Silicon Films Grown by Disilane-Based Low-Pressure Chemical Vapor Deposition. J. Electrochem. Soc. 144, 3952–3958. https://doi.org/10.1149/1.1838117

Haase, F., Hollemann, C., Schäfer, S., Merkle, A., Rienäcker, M., Krügener, J., Brendel, R.,

Peibst, R., 2018. Laser contact openings for local poly-Si-metal contacts enabling 26.1%-efficient POLO-IBC solar cells. Sol. Energy Mater. Sol. Cells 186, 184–193. https://doi.org/10.1016/j.solmat.2018.06.020

Iqbal, Z., Vepřek, S., 2000. Raman Scattering from Hydrogenated Microcrystalline and Amorphous Silicon. J. Phys. C Solid State Phys. 15, 377–392. https://doi.org/10.1088/0022-3719/15/2/019

Joubert, P., Loisel, B., Chouan, Y., Haji, L., 1987. The Effect of Low Pressure on the Structure of LPCVD Polycrystalline Silicon Films. J. Electrochem. Soc. 134, 2541–2545. https://doi.org/10.1149/1.2100239

Kamins, T., 1998. Polycrystalline Silicon for Integrated Circuits and Displays. Springer US. https://doi.org/10.1007/978-1-4615-5577-3

Kamins, T.I., 1971. Hall mobility in chemically deposited polycrystalline silicon. J. Appl. Phys. 42, 4357–4365. https://doi.org/10.1063/1.1659780

Langford, J.I., Wilson, A.J.C., 1978. Scherrer after Sixty Years: A Survey and Some New Results in the Determination of Crystallite Size. J. Appl. Cryst 11, 102–113. https://doi.org/10.1107/S0021889878012844

Learn, A.J., Foster, D.W., 1987. Deposition and electrical properties of in situ phosphorus-doped silicon films formed by low-pressure chemical vapor deposition. J. Appl. Phys. 61, 1898–1904. https://doi.org/10.1063/1.338036

Liu, W., Yang, X., Kang, J., Li, S., Xu, L., Zhang, S., Xu, H., Peng, J., Xie, F., Fu, J.H., Wang, K., Liu, J., Alzahrani, A., De Wolf, S., 2019. Polysilicon Passivating Contacts for Silicon Solar Cells: Interface Passivation and Carrier Transport Mechanism. ACS Appl. Energy Mater. 2, 4609–4617. https://doi.org/10.1021/acsaem.8b02149

Madsen, L.D., Weaver, L., 1990. In Situ Doping of Silicon Films Prepared by Low Pressure Chemical Vapor Deposition Using Disilane and Phosphine. J. Electrochem. Soc. 137, 2246–2251. https://doi.org/10.1149/1.2086921

Mandurah, M.M., Saraswat, K.C., Kamins, T.I., 1979. Phosphorus Doping of Low Pressure Chemically Vapor-Deposited Silicon Films. J. Electrochem. Soc. 126, 1019–1023. https://doi.org/10.1149/1.2129167

Meyerson, B.S., Olbricht, W., 1984. Phosphorus-Doped Polycrystalline Silicon via LPCVD: I. Process Characterization. J. Electrochem. Soc. 131, 2361–2365. https://doi.org/10.1149/1.2115258

Meyerson, B.S., Yu, M.L., 1984. Phosphorus-Doped Polycrystalline Silicon via LPCVD: II. Surface Interactions of the Silane/Phosphine/Silicon System. J. Electrochem. Soc. 131,

2366–2368. https://doi.org/10.1149/1.2115259

Mulder, J.G.M., Eppenga, P., Hendriks, M., Tong, J.E., 1990. An Industrial LPCVD Process for In Situ Phosphorus-Doped Polysilicon. J. Electrochem. Soc. 137, 273–279. https://doi.org/10.1149/1.2086381

Murarka, S.P., 1984. Phosphorus out-diffusion during high temperature anneal of phosphorus-doped polycrystalline silicon and SiO2. J. Appl. Phys. 56, 2225–2230. https://doi.org/10.1063/1.334281

Naber, R.C.G., Van De Loo, B.W.H., Luchies, J.R.M., 2019. LPCVD In-situ N-type Doped Polysilicon Process Throughput Optimization and Implementation into an Industrial Solar Cell Process Flow, in: 36th European Photovoltaic Solar Energy Conference and Exhibition. pp. 180–183. https://doi.org/10.4229/EUPVSEC20192019-2BO.3.2

Padhamnath, P., Khanna, A., Nandakumar, N., Nampalli, N., Shanmugam, V., Aberle, A.G., Duttagupta, S., 2020. Development of thin polysilicon layers for application in monoPoly^{TM} cells with screen-printed and fired metallization. Sol. Energy Mater. Sol. Cells 207. https://doi.org/10.1016/j.solmat.2019.110358

Steinkemper, H., Feldmann, F., Bivour, M., Hermle, M., 2015. Numerical Simulation of Carrier-Selective Electron Contacts Featuring Tunnel Oxides. IEEE J. Photovoltaics 5, 1348–1356. https://doi.org/10.1109/JPHOTOV.2015.2455346

Xiao, C., 2020. Taking TopCON to Top Runner: Jolywood president Lin Jianwei talks solar n-type cell innovation - PV Tech [WWW Document]. URL https://www.pv-tech.org/taking-topcon-to-top-runner-jolywood-president-lin-jianwei-talks-solar-n-type-cell-innovation/ (accessed 7.15.21).

Yan, D., Cuevas, A., Michel, J.I., Zhang, C., Wan, Y., Zhang, X., Bullock, J., 2021. Polysilicon passivated junctions: The next technology for silicon solar cells? Joule. https://doi.org/10.1016/j.joule.2021.02.013